

Electrochemical Optical, and Impedance Studies on Photoactive Assembles Consists of Mixed TiO₂-CdS Particles Occluded in Poly 2,2' Bithiophene in Orthoorthophosphate and Citrate Electrolytes. Part II.

Kasem K. Kasem^{}, Sarah H. Osman, Joshua Jarrett, and Monica Shultz*

School of Sciences, Indiana University Kokomo, Kokomo, IN, USA

*E-mail: kkasem@iuk.edu

Received: 22 June 2020 / Accepted: 28 July 2020 / Published: 30 November 2020

Amorphous nanoparticles of 50/50 TiO₂/CdS mixtures were prepared and immobilized in poly 2,2-bithiophene (PBTh) by occlusion electrodeposition. The photoelectrochemical (PEC) and impedance studies were performed in aqueous orthoorthophosphate and citrate electrolytes. Similar studies were also performed on pure amorphous cadmium sulfide (CdS) and titanium oxide (TiO₂). Photoelectrochemical (PEC) studies revealed evidence of hole accumulations at the interfaces. Furthermore, PEC studies indicated that occlusion of CdS/TiO₂ mixtures, prepared by mechanical mixing, in PBTh gave greater photocurrents than films of PBTh occluded with codeposited CdS/TiO₂ mixtures. Transient time constant studies indicate that orthophosphate anions reduced the rate of electron-hole (e-h) recombination more than citrate, and further enhanced the generated photocurrent. Electrochemical impedance spectroscopic studies (EIS) revealed that occluded assembly films possess a porous-type structure, with multiple phases as indicated by the generation of Nyquist plots with composite semi-circles. The study also shows that orthophosphate anions enhanced the photoactivities at these interfaces more than citrate did. The studied assemblies showed photostability during a prolonged period for of illumination. The long photocurrent transient time recorded for these assemblies recommend it for potential energy capture and storage devices.

Keywords: CdS-TiO₂ mixtures, photoactive interfaces, optical, organic semiconductors, impedance

1. INTRODUCTION

The diffuse nature [1] of organic semiconductor's highest occupied molecular orbitals (HOMO) and lowest unoccupied molecular orbitals (LUMO) qualifies them for coupling with inorganic semiconductors (SC) to widen the absorption range. This coupling would allow formation of hybrid materials with a large surface area interface. Success in sensitizing large bandgap inorganic SCs would

lead to further development of functional hybrid materials. With equal importance to this functional hybrid materials assembly is the electrolyte component in the photoactive interface. The activity of a photoactive interface depends on the electrolyte used. This is important to enhance the kinetics of O₂ evolution on the photoanode surface during photolysis in aqueous electrolytes. The presence of some ions in the aqueous solutions can lead to depletion of photo-generated holes and inhibit O₂ evolution. For this reason, investigation of the same photoactive interface in different electrolytes can lead to identifying the conditions that produce the maximum photochemical outcome and maintain the long-term stability of the interface. Photo-oxidation of anions in the aqueous solution of supporting electrolytes can also compete with the photooxidation of water [2-6].

Many applications have been reported about the use of solar energy in the oxidation of water. Perovskite based solar cells that used CH₃NH₃PbI₃ generated 12.3% conversion efficiency [7]. Several photoelectrochemical studies were performed in aqueous electrolytes containing Ferri/Ferro cyanide [8-10], sulfates [11], and acetate [12] to name but a few. The donor/accepter role of electrolyte ions in the PEC behavior of photoactive p or n type organic SC has been investigated [13-16].

In this paper, we studied the PEC and EIS at the interface of a hybrid assembly made of TiO₂-CdS occluded in PBTh, in the presence of orthophosphate and in citrate aqueous electrolytes. We chose orthophosphate ion as a stable inorganic anion used in many buffer solutions, and citrate anion as an example of organic polycarboxylic anion. The objective is to examine how the electrolyte anion affects the PEC outcome and the dielectric properties of the interface made by the hybrid assembly film and these anions.

2. EXPERIMENTAL

2.1. Reagents

The monomer 2,2- bithiophene (BTh) (Alfa Aesar) was used to prepare poly 2,2 bithiophene (PBTh). Titanium oxide (TiO₂), cadmium sulfide (CdS), Lithium perchlorate (LiClO₄), citrate, and other reagents orthophosphate salts used were of analytical grade. Unless otherwise stated, all of the solutions were prepared using deionized (DI) water.

2.2 Preparations

TiO₂ nanoparticles were prepared as previously described [17]. TiO₂ sensitized with CdS (TiO₂/CdS codep.) was prepared following a modified synthesis procedure previously published (30, 31). CdS was prepared as previously described [18]. A mechanical mixture of TiO₂ and CdS (TiO₂/CdS mec) was prepared as follows: 0.5 g of CdS nanoparticles were dispersed in Titanium iso-propoxide (in 80% ethanol) and stirred for 4 hours. The pale yellowish deposit was collected, washed and dried at 120 °C for 6 hours. inorganic/organic interface (IOI) assemblies thin films were prepared using the occlusion method; thin films of each of TiO₂-CdS, CdS or TiO₂ occluded in PBTh were generated electrochemically using cyclic voltammetry (CV) by scanning the potential of FTO electrode between

-0.5 and 1.7 V vs Ag/AgCl in a suspension (1 mg/mL) of the inorganic materials in acetonitrile containing 5 mM of the BTh monomer and 0.5 M LiClO₄.

2.3. Instrumentation

A conventional three-electrode cell consisting of a Platinum (Pt) wire as a counter electrode, a Ag/AgCl reference electrode, and FTO with surface area 2.0 cm² was used as the working electrode for electrochemical studies. Photoelectrochemical studies of the thin solid films were performed using the experimental setup as described in previous work [12, 19]. A Solartron 2101A was used for the electrochemical impedance spectroscopy (EIS) studies in a frequency range between 0.01 to 100 KHz. A BAS 100W electrochemical analyzer (Bioanalytical Co. IN) was used to perform the electrochemical studies. Optical parameters were calculated based on the steady-state reflectance spectra, measured by a Shimadzu UV-2101PC spectrophotometer. An Olympus BX-FL Irradiation was performed with a solar simulator 300-watt xenon lamp (Newport, NJ) with an IR filter. All measurements were performed at 298 K.

3. RESULTS AND DISCUSSION

3.1 Optical band gap structure:

Previously we investigated the optical properties of the materials used in the studied assemblies (20). Some of data are summarized in Table 1, which indicate that occlusion of either TiO₂ or CdS or both in poly bithiophene noticeably decreases the value of Urbach energy band tail. Further, all of the studied assemblies show a direct and indirect band gap structures. The occlusion increases the optical band gap by 0.2 to 0.4 eV.

Table 1. Optical band gap for the studied assemblies.

Assembly	≈ band gap at λ max (eV)	Direct band gap, (eV)	Indirect band gap(eV)	Urbach energy, (eV)
PBTh	2.4	2.0	1.1	0.76
PBTh/CdS	2.6	2.2	1.9	0.07
PBTh/TiO ₂	2.8	2.2	1.9	0.08
PBTh/TiO ₂ -CdS (codep.)	2.8	2.25	1.9	0.125
PBTh/TiO ₂ -CdS (mec.)	2.8	2.2	1.9	0.07

3.2. Photoelectrochemical studies.

Unless otherwise stated, the electrochemical (EC) studies on FTO/PBTh/occluded with each of TiO₂, CdS and CdS-TiO₂ were carried out by cycling the potential of each of FTO/PBTh, FTO/PBTh/CdS-TiO₂, FTO/PBTh-CdS and FTO/PBTh-TiO₂ between -1.0 to 1.0V vs Ag/AgCl in orthophosphate and citrate electrolyte (pH 7.6). Such potential cycling took place in the dark and under illumination at a scan rate 0.100V/s. The results are displayed in Figures 1,2,3, and 4. Figures 1 and 2 clearly indicate that the under illumination, the recorded photocurrent exceeds the current recorded in the dark at approximate 0.3 V vs Ag/AgCl. We consider that as the approximate value of the flat band potential (E_{Fb}). No big differences between E_{Fb} on using orthophosphate or citrate electrolyte was found.

The data listed in Table 2 clearly indicate that occlusion of a mixture of CdS-TiO₂ into PBTh generates more photo current than the native PBTh. The mechanical mixture of CdS-TiO₂ generates more photocurrent than the codeposited mixture. The occluded PBTh produced more photocurrent in a orthophosphate electrolyte than that in citrate electrolyte. The occlusion of only TiO₂ in PBTh generate greater photocurrent than that observed when occluded with CdS. This suggests that the TiO₂ in the mixture was the major contributor to the increase in the photocurrent.

Table 2. Photocurrent (I photo-I dark) generated for the listed assemblies in 0.2M of orthophosphate and of citrate electrolytes (pH 7.6).

Assembly	Generate Photocurrent, at -.850 V vs Ag/AgCl, (μ A)	
	Orthophosphate	Citrate
PBTH	80.0	172.7
PBTh/CdS	192	168
PBTh/TiO ₂	319	262
PBTh/TiO ₂ -CdS (codep.)	281	176
PBTh/TiO ₂ -CdS (mec.)	353	309

The CV displayed in Figures 1 and 2 also represent the electrode chemical capacitance or density of state (DoS) of these organic semiconductors' assemblies. The following equation illustrates the relationship [21].

$$p(E) = \frac{1}{eAd} \int \frac{idE}{s} \quad 1$$

where $p(E)$ is DoS in the potential range dE , e is electron charge, A is electrode surface area, d is film thickness, I is current at given potential, and s is the scan rate V/s .

Figures 1 and 2 show the approximate onset oxidation potentials of the studied assemblies is 0.7 V vs Ag/AgCl or at 5.5 eV (in vacuum scale). This is also the approximate position of HOMO. The approximate position of LUMO would be at -1.3 V vs Ag/Agcl. The calculate $p(E)$ near the LUMO bands is in the range of $1.0 - 1.9 \times 10^{20} \text{ cm}^{-3}$. This depends on the materials occluded into the PBTh film. Figures 1 and 2 display the CV for PBTh/CdS-TiO₂ (codeposition) mixture only because the CV for the PBTh/CdS-TiO₂ mechanical mixture was similar to that of the PBTh/CdS-TiO₂ (codeposition) mixture. The CV of the occluded PBTh is similar but not identical to that reported [20] for unoccluded PBTh. The differences that occlusion caused are illustrated in the data listed in Tables 2 and 3.

The observed photo-current shows evidence of hole accumulations. This is clearly shown in Figures 3 and 4 in which the photocurrent-time plot for all studied assemblies are displayed. It is worth notice a sharp anodic current spike is observed during illumination of any of the occluded assemblies. This phenomenon was reproducible.

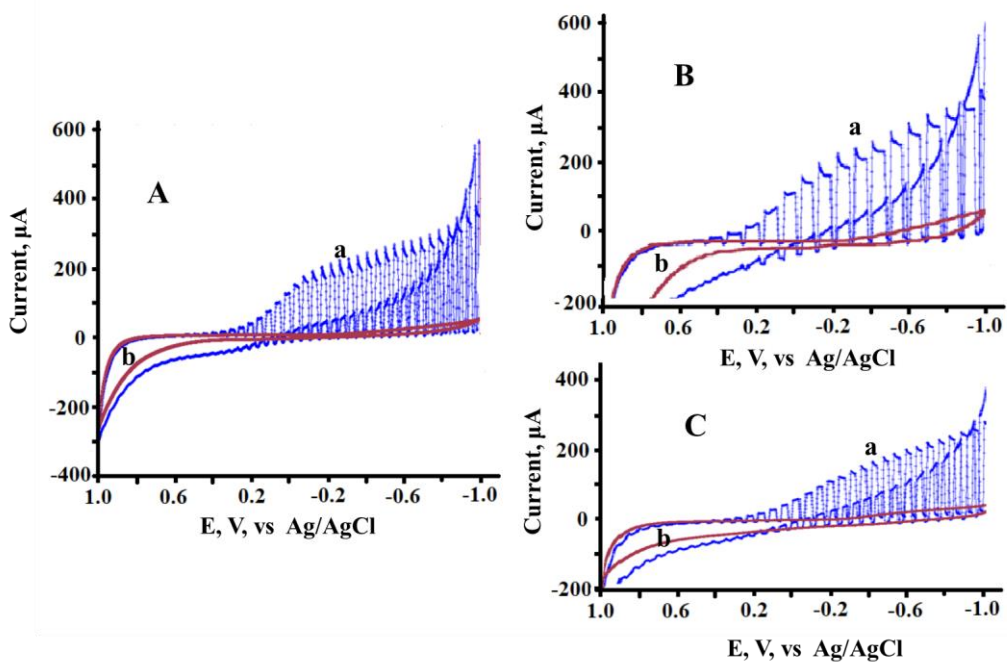


Figure 1 CV in 0.2 M orthophosphate electrolyte (pH 8) at 0.10V/s: a) under illumination, and b) dark; **A)** of FTO /PBTh/CdS-TiO₂(Codep.), **B)** FTO/PBTh/TiO₂, and **C)** FTO/PBTh/CdS

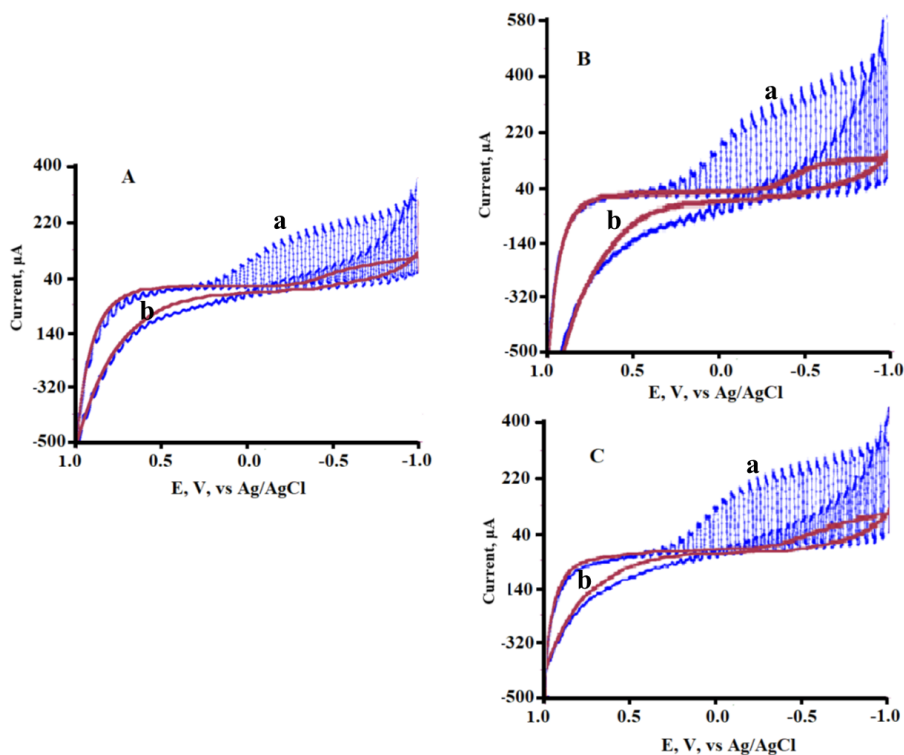


Figure 2. CV in 0.2 M citrate electrolyte (pH 8) at 0.10V/s: a) under illumination, and b) dark; **A)** of FTO /PBTh/CdS-TiO₂(Codep.), **B)** FTO/PBTh/TiO₂, and **C)** FTO/PBTh/CdS

This is evidence of a fast charge recombination due to the hole accumulations (22) at the assembly's upper layer/electrolyte interface. Such behavior was not observed for FTO/PBTh. Furthermore, under darkness, no backflow of electrons from the substrate FTO to the assembly body took place. The lack of cathodic current (reversed transient current) is evidence for the lack of backflow of electrons.

3.3. Hole accumulation phenomena:

The sudden increase in photocurrent upon illumination shown in Figures 3 and 4 can be explained on the basis of the existence of hole accumulation in the mixed phases of the organic polymers. The p-type nature of organic semiconductor's polymers lead to hole accumulations. When a p-p type heterojunction is created, possible hole accumulation can take place. The concentration of these hole accumulations and the transient current time constant can be quantitatively calculated.

The concentration of accumulated holes was calculated (Table 3) by integrating the area under each of spike with consideration of the charge density and photochemical equivalence law.

Furthermore, considering the following equation (23).

$$R = e^{-\frac{t}{\tau}} \tag{2}$$

Where t , time, τ is transient time constant and $R = (I_t - I_{st}) / (I_{in} - I_{st})$, as I_t is current at time t , I_{in} is immediate photocurrent, and I_{st} is the stationary value of photocurrent (steady current).

The plot of $\log R$ vs time, generates a straight line with slope = $1/\tau$. The reciprocal of the slope determines the value of τ , in seconds.

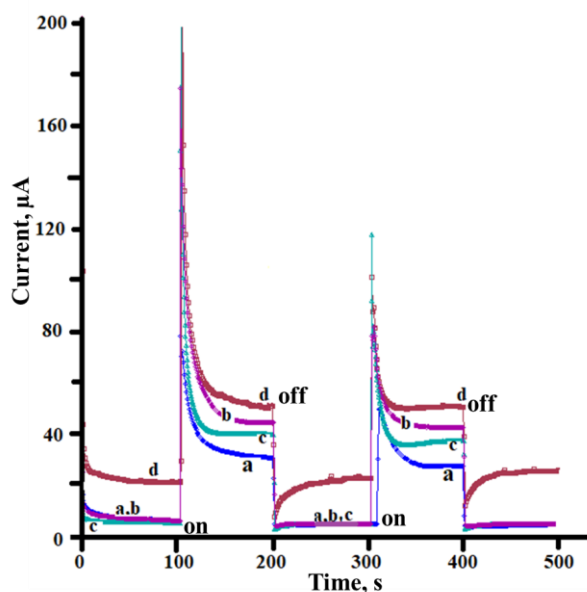


Figure 3. a-PBTh/CdS, b-PBTh/TiO₂, c- PBTh/TiO₂-CdS (Codeposition), and d- PBTh/TiO₂-CdS(mec mix.) in 0.2M orthophosphate electrolyte.

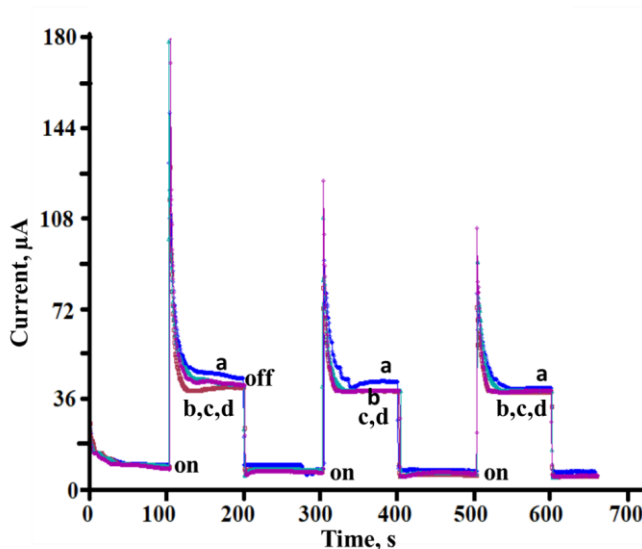


Figure 4. a- PBTh/CdS, b-PBTh/TiO₂, c- PBTh/TiO₂-CdS (Codeposition), and d-PBTh/TiO₂-CdS (mec. mix.) in 0.20 M citrate electrolyte.

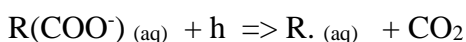
Table 3. Hole accumulation concentration and photocurrent transient time constants τ and s , generated by phases created with interface FTO/PBTH/CdS/TiO₂

System	Orthophosphate		Citrate	
	τ (sec.)	[Hole] (mole)/cm ²	τ (sec.)	[Hole] (mole)/cm ²
PBTh	2.55	6.2×10^{-9}	2.19	3.58×10^{-10}
PBTh/CdS	8.62	3.8×10^{-9}	5.82	5.9×10^{-9}
PBTh/TiO ₂	7.75	9.2×10^{-9}	4.72	7.18×10^{-9}
PBTh/Mix*/codep.	8.2	7.0×10^{-9}	4.59	3.98×10^{-10}
PBTh/Mix/mec.	5.26	7.6×10^{-9}	5.38	5.8×10^{-9}

* Mix = TiO₂-CdS

The data listed in Table 3 clearly indicate that a greater transient time constant is recorded for the occluded PBTh with either CdS or TiO₂ or both than for the native PBTh. This means that occlusion slows the electron–hole recombination rate and enhances charge separation and charge transfer. Table 3 also indicate that the transient time constant in orthophosphate is longer than that in citrate. Furthermore, in citrate, occluded PBTh possesses greater hole concentration than the un-occluded film. This trend was also observed in orthophosphate but to a lesser extent. This highlights the role of the electrolyte anions on the photochemical activities at the electrode/electrolyte interface, indicating that orthophosphate ions contributed to slowing the rate of the e-h recombination process.

Previous studies [24] show that orthophosphate ions adsorbed at the photoactive interface can be oxidized to form [PO₄⁻]. For organic anions containing carboxylic group (COO⁻) can react with holes to generate CO₂ according to the following reaction [25]:



However, in presence of multi COO^- groups as in citrate anions, the hole consumption would be more complex than that illustrated in reaction 3. Hole consumption by orthophosphate may have contributed to slower e-h recombination in orthophosphate electrolyte than that in citrate electrolyte.

3.4. Electrochemical Impedance studies:

Impedance complexes (Nyquist plot) generated in the dark and under illumination from assemblies a) PBTh/CdS, b) PBTh/TiO₂, c) PBTh/CdS-TiO₂ (codepos.), and d) PBTh/CdS-TiO₂ (Mech.) on FTO substrate are displayed in Figures 5 (in citrate electrolyte) and in Figure 6 (in orthophosphate electrolyte). It can be notice that at all frequencies, only kinetic control is observed. Under illumination, the generated Nyquist plots show composite semi-circles (Figures 5A and 6A). This is evidence that the assembly films possess a porous-type structure, with multiple phases. The dielectric behavior of the generated assemblies was explored at 25°C by further treatment of EIS data for each of the studied assemblies. The AC conductivities (σ_{ac}) of these assemblies in orthophosphate and in citrate electrolytes was determined using the following equation [26]

$$\sigma_{ac} = \frac{L}{a} * \frac{Z'}{Z'^2 + Z''^2} \quad 4$$

As L is film thickness, and a is electrode surface area (2.0 cm²)

The relation between σ_{ac} and DC conductivity (σ_{dc}), is illustrated in the following universal dynamic response (UDR) formula or Jonscher's power law [27].

$$\sigma_{ac} = \sigma_{dc} + A\omega^s \quad 5$$

where A is the strength of polarizability and s is temperature-dependent parameter which can be determined from the plot of $\log \sigma_{ac}$ vs $\log \omega$.

$$\log \sigma_{ac} = \log \sigma_{dc} + \log A + s \log \omega \quad 6$$

From the plot of $\log \sigma_{ac}$ vs $\log \omega$, we determined the slope s using the power law. Hopping frequency (ω) and relaxation time (τ in seconds) were determined for all studied assemblies (data not shown). The exponent, s, in the power law is important in the determination of the potential barrier separating defect centers in the pass of charge carriers (W_m).

W_m can be calculated from the following relationship [28] :

$$W_m = \frac{6k_B T}{1-s} \quad 7$$

The values of s must be ≤ 1 to generate positive W_m value according to Equation 7. Tables 4 and 5 list the exponent (s), barrier energy (W_m), hopping frequency (ω_{hopping}), minimum hopping distance (R_{min}) and density of state at Fermi level $N(E_F)$ at high frequency calculated for all of the studied assemblies. Table 4 shows that occlusion in PBTh decreased the values of s, W_m ,

ω_{hopping} , and $N(E_F)$ compared to that calculated in PBTH only. Results show that only R was increased in the occluded PBTh. Table 4 also shows that, under illumination, the s, W_m , ω_{hopping} and $N(E_F)$ are less than those determined in the dark. Only R values increased under illumination. On the other hand, table 5 show that, in orthophosphate electrolyte, a trend similar to that observed in citrates in dark, however the illumination increased both $N(E_F)$ and ω_{hopping} . Tables 4 and 5 indicate that the exponent (s), the barrier energy (W_m) and $N(E_F)$ in citrate are greater than those determined in

orthophosphate. This is contrary to the R where the calculated values of R in citrates are less than those calculated in orthophosphate.

As s was considered as a function of entropy [27], the lower the value of s, the greater the entropy or the disorder of molecules or segments in the interface between different microstructure (heterogeneity) of this interface. The exponent s is then a function of movement of the segments. Decreasing s upon illumination indicates increasing entropy. Illumination created excited states and more random motion within the illuminated interfaces. The data listed in Table 4 and 5 suggest that orthophosphate anions enhanced the photo-activities at these interfaces more than citrate did. Furthermore, occlusion of mechanical mix of CdS-TiO₂ increased N(E_F) and W_m than the CdS-TiO₂ prepared by the codeposition method.

Table 4. Exponent s, Barrier energy W_m, hopping frequency (ω_{hopping}), minimum hopping distance (R_{min}) and density of state at Fermi level N(E_F) at high frequency in citrate electrolyte.

Phase	Dark					Light				
	s	W _m (eV)	N(E _F)	ω (KHz)	R _{mi} (nm)	s	W _m (eV)	N(E _F)	Ω (KHz)	R _{min} (nm)
Poly BTh	0.962	4.053	5.24 x10 ²⁰	2.82	0.2	0.507	0.3124	5.91x10 ²⁰	6.02	2.3
BTh/CdS	0.664	0.458	1.16x10 ²⁰	5.01	2	0.443	0.276	5.70x10 ¹⁹	3.16	3.0
BTh/TiO2	0.760	0.642	1.96x10 ²⁰	5.01	1.5	0.700	0.513	1.21x10 ²⁰	2.82	1.9
BTh/Mix(code)	0.649	0.439	9.1x10 ¹⁹	3.98	2.2	0.553	0.345	5.61x10 ¹⁹	3.16	2.8
BTh/Mix(mec)	0.791	0.737	4.33 x10 ²⁰	3.98	1.1	0.600	0.385	1.37x10 ²⁰	1.37	2.0

Table 5. Exponent (s), Barrier energy (W_m), hopping frequency (ω_{hopping}), minimum hopping distance (R_{min}) and density of state at Fermi level N(E_F) at high frequency in orthophosphate electrolyte.

Phase	Dark					Light				
	s	W _m ,eV	N(E _F)	ω , (KHz)	R _{min} , (nm)	s	W _m ,eV	N(E _F)	ω , (KHz)	R _{min} , (nm)
Poly BTh	0.750	0.613	2.52x10 ²⁰	0.631	1.4	0.731	0.570	2.21x10 ²⁰	0.631	1.5
BTh/CdS	0.287	0.216	3.58x10 ¹⁹	12.02	3.8	0.292	0.218	3.55x10 ¹⁹	10.0	3.8
BTh/TiO2	0.121	0.175	1.46x10 ¹⁹	5.62	5.5	0.280	0.194	1.86x10 ¹⁹	15.85	4.9
BTh/Mix(Cod)	0.295	0.202	2.02x10 ¹⁹	8.91	4.7	0.454	0.282	3.83x10 ¹⁹	16.60	3.4
BTh/Mix(mec)	0.651	0.441	1.96 x10 ¹⁹	6.31	1.7	0.454	0.282	7.65x10 ¹⁹	17.78	2.7

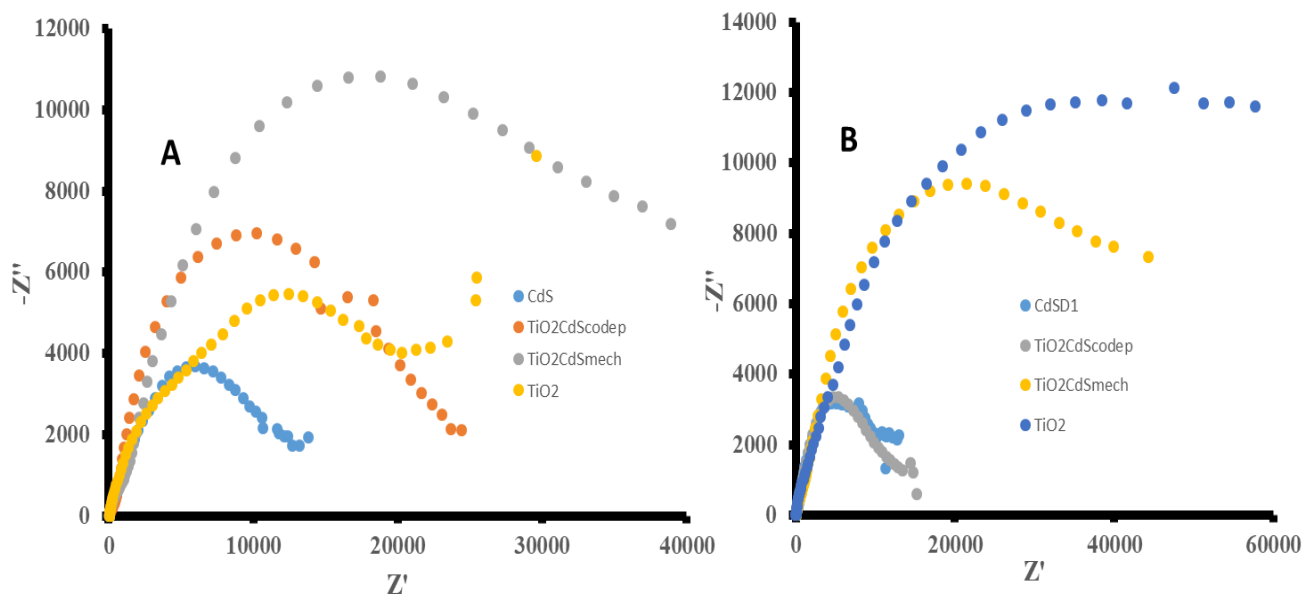


Figure 5. Nyquist plot at -0.50 V vs Ag/AgCl in citrate electrolyte (pH 7.6) for a) PBTh/CdS , b) PBTh/TiO₂, c) PBTh/CdS-TiO₂ (codep.), and d) PBTh/CdS-TiO₂ (mec.) in A) Light, in B) dark

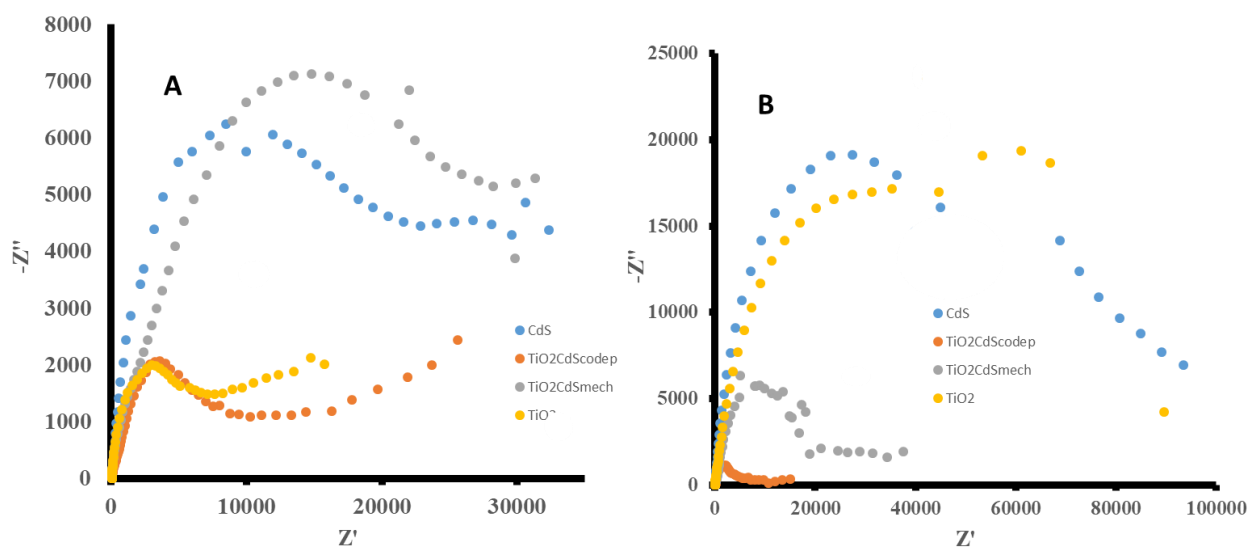


Figure 6. Nyquist plot at -0.50 V vs Ag/AgCl in orthophosphate electrolyte (pH 7.6) for a) PBTh/CdS , b) PBTh/TiO₂, c) PBTh/CdS-TiO₂ (codep.) , and d) PBTh/CdS-TiO₂ (mec.), in A) Light, in B) dark

3.5. Anion effect

The effect/s of electrolyte anions at the photoactive interface can be tracked by it's effect on the structure of the double layer at the electrode /electrolyte interface.

The net electrostatic effect of a charge carrier in a solution can be correlated to Debye length (λ). Such length can be calculated using the following equation [29] :

$$\lambda = \sqrt{\frac{\epsilon_r \epsilon_0 k_B T}{z * 2000 N_A e^2 I}} \quad 8$$

As, I is the ionic strength of the electrolyte (mol/L), ϵ_0 is the permittivity of free space, ϵ_r is the dielectric constant, k_B is the Boltzmann constant, T is the absolute temperature, N_A is the Avogadro's number, e is the elementary charge, and Z is the anion charge.

Using the dielectric values obtained from impedance studies at very low frequencies at 298K, λ was calculated and listed in Table 6

Table 6. Debye length (nm) at the illuminated interfaces in different anions

System	Citrate $C_4H_6O_3(COO)_2^{2-}$	Orthophosphate HPO_4^{2-}
PBTh	2.2	2.2
PBTh-CdS	4.1	5.7
PBTh-TiO ₂	3.9	3.6
PBTh/TiO ₂ -CdS/ (codep)	2.4	2.5
PBTh/TiO ₂ -CdS (mec)	2.6	2.7

The data listed in Table 6 shows that occlusion increased double layer (Debye length) thickness, and consequently increased the shielding distance. The role of the double layer could have affected the involvement of electrolyte anions in the photoelectrochemical process. The anions adsorbed over the photoactive interface can participate in a catalytic aerobic redox process. The mechanism of charge (hole or electron) participation can occur either by indirect injection of photoexcited hot hole to the anion, or by direct injection of surface charge [30]. The fact that all studies were performed in oxygenated electrolytes, suggests that O₂ mediated the photo-electrochemical reaction through intermediate step by which a surface plasmon induces hot electron –injection into an O₂ molecule [31]. Figures 3 and 4 indicate that orthophosphate electrolytes generated more photocurrent than citrates electrolytes. Furthermore, Table 3 indicates that hole accumulation at the orthophosphate/electrode interface is generally greater than that at the citrate interface. The hole transfer may explain why the photo electrochemical response is greater in orthophosphate than in citrate. The structure of orthophosphate anion explains its greater, permanent inductive effect than citrate anion which possess greater but temporary electromeric effect due to the larger number of π bonds. Inductive effect is important factor that enhance charge separation and consequently greater photocurrent.

5. CONCLUSION

The observed PEC and impedance behavior of the assemblies FTO/ PBTh, occluded with CdS-TiO₂ indicates that the interface with the electrolyte was the dominant contributor to the recorded outcome. The evidence of hole accumulation left no doubt that interaction took place between the

electrolyte anions and holes accumulated at the outermost layers of the assembly. No evidence was reported for reversed transient current that reflected any backflow of electrons from the FTO as a substrate to the body of the assembly. Our studies show that orthophosphate anions were more effective than citrate anions in interaction with the holes accumulated at the outermost layers of the assemblies.

ACKNOWLEDGMENT

The authors acknowledge Office of the Academic Affairs at Indiana University Kokomo for supporting this project.

References

1. M. Oehzelt, N. Koch and G. Heimel, *Nat. Commun.*, 5 (2014) Article number: 4174 .
<https://doi.org/10.1038/ncomms5174>.
2. Q. Mi, A. Zhanaidarova, B. S. Brunschwig, H.B Gray, N.S. Lewis, *Energy Environ. Sci.*, 5 (2012) 5694.
3. R. Liu, Y. Lin, Y. L. Chou, S. Sheehan, W. He, F. Zhang, H. Hou, D. Wang, *Angew. Chem., Int. Ed.*, 50 (2011) 499.
4. G. Wong, Y. Ling, H.Wang, X.Yang, C.Wong, J. Zhang, Y. Li, *Energy Environ. Sci.*, 5 (2012) 6180.
5. CRC Handbook of Chemistry and Physics, 81st ed.; CRC Press: Boca Raton, FL, 2000. (24) Pourbaix, M. Atlas of Electrochemical Equilibria in Aqueous Solutions; National Association of Corrosion Engineers: 1974.
6. J. C. Hill and Kyoung-Shin Choi. *J. Phys. Chem. C*, 116 (2012) 7612.
7. Jingshan Luo, Jeong-Hyeok Im, Matthew T. Mayer, Marcel Schreier, Mohammad Khaja Nazeeruddin, Nam-Gyu Park, *Science*, 345 (6204) (2014) 1593, DOI: 10.1126/ science.1258307.
8. T. Daeneke Y. Uemura, N. W. Duffy A. J. Mozer N. Koumura U. Bach , L. Spiccia, *Adv. Mater.*, 24(2012) 1222.
9. M. Zagorska, H. Wycislik, J. Przyluski, *Synth. Met.*, 20 (1987) 259.
10. M. Tolgyesi, A. Szucs, C. Visy, M. Novak, *Electrochim. Acta*, 40 (1995) 1127.
11. T. Bak, J. Nowotny, M.Rekas, C.C. Sorrell, *Int. J. Hydrogen Energy*, 27 (2002)19.
12. K. Kasem, H. Worley and M. Elmasry, *Adv. Compos. Hybrid Mater.*, 2018;
<http://doi.org/10.1007/s42114-018-0055-0>
13. M. A. Carlo A, Bignozzi, T. A. Heimer, G. M. Hasselmann, G. J. Meyer, *J. Phys. Chem. B*, 102 (1998) 7577.
14. Jian-Ke Sun, P. Wang, Qing-Xia Yao, Yong-Juan Chen, Zhao-Hui Li, Yong-Fan Zhang, Li-Ming Wua and Jie Zhang, *J. Mat. Chem.*, 24 (2012) 12212.
15. M. Bates and R. R. Lunt, *Sustainable Energy Fuels*, 1(2017)955.
16. C. Minero, G. Mariella, V. Maurino, E. Pelizzetti, *Langmuir*, 16 (6) (2000) 2632.
17. Hsiao-Yen Lee and Girish M. Kale, *Int. J. Appl. Ceram. Technol.*, 5 (6) (2008)657,
DOI:10.1111/j.1744-7402.2008.02248.x
18. Z. R. Khan, M. Z. Mohd. S. Khan, *J. Mat. Sci.*, 46 (2011) 5412.
19. K. Kasem, M. , Elmasry, K. Baker, and C. Santucci, *Thin Solid Films*, 634 (2017)56.
20. K. Kasem, S. H. Osman, A.J. Wayn, *Int. J. Electrochem. Sci.*, 11 (2019). doi: 10.20964/2019.12.58.
21. Damian Monllor-Satoca and Roberto Gomez, *J. Phys. Chem.C*. 117 (2008) 139.
22. M. Sookhakian , Y.M. Amin, S. Baradaran, M.T. Tajabadi, A. Moradi Golsheikh, and W.J. Basirun, *Thin Solid Films*, 552 (2014) 204.
23. F.Spadavecchia , S. Ardizzone , G. Cappelletti, L. Falciola, M. Ceotto, D. Lotti, *J. Appl*

- Electrochem.*, 43 (2013) 217. <https://doi.org/10.1007/s10800-012-0485-2>.
24. M. Abdullah, G K. C. Low, R.W.Matthews, *J. Phys Chem.*, 94 (17) (1990) 6820.
 25. R.M. Cerviño , W.E.Triaca, A.J. Arvía, *J. Electroanal Chem.*, 172 (1984) 255.
 26. J.H. Joshia, D.K. Kanchan, J.M. Joshi, H.O. Jethva. *Mater. Res. Bull.*, 93(2017)63.
 27. A.K. Jonscher. *Nature*, 267 (1977) 673, DOI 10.1038/26763a0.
 28. K. Funke, *Prog. Solid. State Chem.*, 22(1993)111.
 29. W.B. Russel, D.A. Saville, and W. R. Schowalter, *Colloidal Dispersions*, Cambridge University Press, 1989
 30. E. S. Thrall, A. P. Steinberg, Xi. Wu, L. E. Brus, *J. Phys. Chem. C*, 117 (49) (2013) 26238.
 31. Liu-Bin Zhao, Xiao-Xiang Liu, Meng Zhang, Zi-Feng Liu, De-Yin Wu, Zhong-Qun Tian, *J. Phys. Chem. C*, 120 (2) (2016) 944.

© 2021 The Authors. Published by ESG (www.electrochemsci.org). This article is an open access article distributed under the terms and conditions of the Creative Commons Attribution license (<http://creativecommons.org/licenses/by/4.0/>).